Applied surface science. 2011, vol. 258, issue 5, p. 1862-1868. http://dx.doi.org/10.1016/j.apsusc.2011.10.063

Possible stibnite transformation at the friction surface of the semi-metallic friction composites designed for car brake linings

V. Matějka [a,*], Y. Lu[b], P. Matějková[c], B. Smetana[d], J. Kukutschová[a], M. Vaculík [a], V. Tomášek[a], S. Zlá[d], Y. Fan[b]

[a] Nanotechnology Centre, VŠB-Technical University of Ostrava, 17. listopadu 15/2171, 708 33 Ostrava-Poruba, Czech Republic.

[b] The Key Laboratory of Beijing City on Preparation and Processing of Novel Polymer Materials, Box 82, Beijing University of Chemical Technology, Beijing 100029, PR China.

[c] CPIT, VŠB - Technical University of Ostrava, 17. listopadu 15/2172, 708 33 Ostrava, Czech Republic.

[d] Department of Physical Chemistry and the Theory of Technological Processes, VŠB-Technical University of Ostrava, 17. listopadu 15/2172, 708 33 Ostrava-Poruba, Czech Republic.

Introduction:

After a friction process several changes in phase composition of friction composites are often registered. High temperature, accompanied by high pressure induced during braking can cause initiation of chemical reactions which do not run at room or elevated temperatures under the atmospheric pressure. Most of the studies in the field of tribochemistry at friction surfaces of car brake linings deal with phenolic resin degradation and corrosion of metallic components. In this work we describe the formation of elemental antimony as well as the alloying process of iron with antimony observed on the surface of laboratory prepared semi-metallic friction composites containing stibnite. The role of alumina abrasives in the process of stibnite transformation is also discussed.

Keywords:

Semi-metallic friction composite, tribochemistry, stibnite, antimony.

*Corresponding author. Tel.: +420 597 321 519; fax: +420 597 321 640.
E-mail address: vlastimil.matejka@vsb.cz (V. Matějka)

Introduction:

Semi-metallic friction composites are commonly used in the manufacturing of car brake linings. There are several reports providing comprehensive review on the formulation and the preparation of the friction composites suitable for car brake lining manufacturing [1, 2, 3, 4]. The components used in formulations of friction composites can be divided into four basic groups: i) binders (e.g. phenolic resin), ii) abrasives (zircon, alumina …), iii) fillers

(barite, calcite, different nut shells …) and iv) functional fillers (e.g. solid lubricants - metal sulfides, graphite). The required functionality of the given friction composite is closely related to the proper selection of components from these four groups. The metallic ingredients increase wear resistance, hardness of composites and improve their thermal diffusivity, and also play an important role in the formation of primary contact plateaus. These plateaus are in direct contact with the rotating counterpart (typically cast iron disc) and transfer the pressure (typically 1,2 MPa during soft braking and 10 MPa in extreme situations) which originates during the braking. The pad covers approximately 10% of the corresponding rubbing surface, and contact plateaus cover typically 15-20% of a brake lining surface [5]. The function of the braking counterparts is to decelerate the velocity of a vehicle, whereas the kinetic energy of rotor is transferred into thermal energy what is reflected in the increasing of the temperature of both braking counterparts. The rotating disc is intermittently in contact with the lining during braking and its temperature rarely reaches values higher than 400°C [6]. On the other hand the brake pad is in contact with the rotating disc during the braking, and the local overheating of the friction surface can rise to a considerably higher temperature than is the mean temperature of a cast iron rotor.

The high temperature on the friction surface, together with the direct, sliding contact of the brake lining with the rotor are responsible for mechanochemical reactions, in this case the tribochemical reactions, which occur during braking. Due to the complex composition of brake linings (common friction composites contain typically 7-20 ingredients) it is difficult to describe all tribochemical reactions in detail. A typical phenomenon occurring at lower temperatures is a degradation of phenolic resin. The onset temperature of phenolic resin degradation is dependent on its nature, modification, and presence of metals which act as catalysts for its degradation [7]. Other reported tribochemical reactions comprise oxidation of metallic components, e.g. iron or copper [8].

Stibnite (Sb_2S_3) and molybdenite (MoS_2) are the most common solid lubricants used in friction composites designed for car brake lining applications, and their effect on friction-wear performance is described in a number of research works e.g. in [9, 10, 11]. The melting point of Sb_2S_3 is 550°C and for MoS_2 is 1185°C. In the presence of oxygen Sb_2S_3 undergoes an oxidation process, whereas at lower oxygen concentration Sb_2O_3 originates while in an oxygen rich environment Sb_2O_4 is formed. In addition to the oxygen concentration, temperature also plays a significant role in the given antimony oxide formation. The oxidation of Sb_2S_3 start to occur in a temperature range between 290 – 340°C when the product of the reaction is Sb_2O_3, at higher temperatures approx. 500°C Sb_2O_4 begins to form. Chemical

equations related to both oxides formation are described by eq. (1a) and (1b), respectively [12].

$$2Sb_2S_3 + 9O_2 = 2Sb_2O_3 + 6SO_2 \quad (1a)$$
$$Sb_2S_3 + 5O_2 = Sb_2O_4 + 3SO_2 \quad (1b)$$

Chemical and phase changes induced by the friction process of the friction composites containing Sb_2S_3 and MoS_2 as the solid lubricants were studied by Filip et al. [13]. The authors did not observe any oxidation of stibnite during the friction process even if the temperature reached 700°C. Kim et al. [14] suggested that formation of antimony oxides at elevated temperatures protect the occurring of the fade phenomenon. If the Sb_2O_3 is formed, its reaction with Sb_2S_3 can occur (2) to form the elemental antimony [12].

$$2Sb_2O_3 + Sb_2S_3 = 6Sb + 3SO_2 \quad (2)$$

Different forms of carbon, mainly graphite, represent common components of friction composites. The content of carbon increases in the friction layer as a result of the organic matter degradation. In the presence of carbon antimony oxides undergo reduction process and metallic antimony can originate; see the reaction (3) for Sb_2O_4 [15]:

$$Sb_2O_4 + 4C = 2Sb + 4CO \quad (3)$$

In semi-metallic friction composites the presence of metals in different forms (chips, wool, and powder) can rise to 50 vol.%. The iron chips or the steel wool are among the most common metallic ingredients. In the presence of iron, and at elevated temperatures, Sb_2S_3 undergoes reaction according to the following reaction scheme (4) [15].

$$Sb_2S_3 + 3Fe = 3FeS + 2Sb \quad (4)$$

Baláž et al. [16] used the reaction (4) for nanosized antimony preparation using high energy ball milling of the mixture of Sb_2S_3 and Fe powder. Using the XRD method, and the measurement of magnetization data, the authors approved completion of reaction (4) after 120 min. long milling.

Recently some authors have mentioned brake pads as a significant source of antimony entering the living environment [17]. Lijima et al. [18] estimated the average emission of antimony in the form of brake dust with particle size characterized as PM2.5 to reach 6.3 ton/year in Japan. Sb_2O_3, as one of the possible antimony compounds entering the living environment, is classified as a compound with possible carcinogenic effect to humans (Group 2B) [19], but there still exists more the hypothesis about its presence in brake dusts than scientific confirmation.

The aim of this work is to study the stibnite transformation on the surface of the semi-metallic friction composites during the friction process, as well as to discuss the effect of alumina abrasives on its transformation.

Experimental details

2.1. Sample preparation

The designed formulations of the semi-metallic friction composite without abrasives assigned as SM_0, and the composite with alumina abrasives assigned as SM_Al, are listed in Table 1.

All the raw materials were mixed using a blender (Electrolux EBR100) for 2 min. After the homogenization the prepared mixture was pressed by the JFY60 molder made by Jilin Wanda Mechanical Co, Ltd. for 6 min at 165°C and 25 MPa. The friction composites were post-cured for 60 min at 120°C, next for 60 min at 150°C, and finally for 120 min at 180°C.

With the aim of describing the changes of stibnite in the presence of iron, the mechanical mixture containing 90 wt.% of iron powder (Lachema) and 10 wt.% of the Sb_2S_3 powder (industrial grade) was prepared by a hand homogenization of the powders using an agate mortar and pestle, and the obtained mixture was assigned as S1. The morphology and particle size distribution of both powders is obvious from the SEM images pictured in Fig. 1.

2.2 Friction performance tests

Friction tests were performed according to the China National Standard GB5763-1998 using the JF151 friction tester (Jilin Wanda Mechanical Co. Ltd) with a constant speed of 500 rpm, a constant pressure 0.98 MPa, a total amount of disc rotations being 5000. The whole test procedure lasted for 10 min. A cast iron disc was used as the rotor, as the stator the prepared friction composites with the size of 25 mm × 25 mm × 6 mm were used. Friction tests were performed at the rotor temperature of 100, 200, 250, 300 and 350°C, and a new friction composite was used for each testing temperature.

2.3 Characterization methods

The friction surfaces of the samples after the friction tests were observed using a scanning electron microscope (SEM) Philips XL30 with energy dispersive X-ray

microanalysis (EDX). The SEM images were obtained using back scattered electrons at an operating voltage of 25 kV.

The X-ray diffraction patterns of the friction surfaces were recorded under CoKα irradiation (λ= 1.789 nm) using the Bruker D8 Advance diffractometer equipped with the fast position sensitive detector VÅNTEC 1. The measurements were carried out in the reflection mode. Phase composition was evaluated using the PDF-2 Release of the 2004 database (International Centre for Diffraction Data).

Differential thermal analysis (DTA) of the mechanical mixture S1 was carried out using a Setaram SETSYS 18TM thermal analyzer and S-type measuring rod. Samples placed in an alumina crucible were analyzed in an argon atmosphere with a heating rate of 10°C min^{-1} from 25°C to i) 350°C; ii) 500°C and iii) 650°C.

3. Results and Discussion:

3.1. Friction performance and SEM study of the friction layer

The graphical presentation of the temperature dependency of coefficient of friction (COF) on the rotor temperature is depicted in Fig. 2. Although the addition of the Al2O3 abrasive increases the value of COF, the trend of COF temperature dependency is very similar for both composites. Decrease in the COF value at a temperature higher than 250°C is connected with degradation of phenolic resin which serves as a binder. Expected stabilization of COF due to the formation of antimony oxides as reported by Jang et al. [9] was not observed.

The character of the friction surface of the samples SM_0 and SM_Al tested at 350°C is shown in Fig. 3a) and Fig. 3b), respectively.

The SEM micrographs of the friction surface of sample SM_0 (Fig. 3a) and SM_Al (Fig. 3b) reveal different character of friction patches. Presence of Al_2O_3 abrasive causes the abrasive character of sliding contact observed on the sample SM_Al to prevail over the adhesive character of sliding contact which is typical for samples without an abrasive.

The raw stibnite particle observed on the friction surface of the sample SM_Al is pictured in Fig. 4a), the EDX spectrum obtained from the area marked by the square is shown in Fig. 4b).

The detail of the friction surface of the sample SM_Al tested at 350°C (in Fig. 3b marked by rectangle and black arrow) is shown in Fig. 5a).

The friction surface presented in Fig. 5a) consists of the areas with different gray scale, that signals a different composition of the patches that occurred on the friction surface of this sample. The EDX spectrum pictured in Fig. 5b) shows the elemental composition of the dark area and revealed the presence of Fe, Sb, S, O, Al and Si. With respect to Fig. 4 the white areas appearing on the friction surface of sample SM_Al (Fig. 3b) are supposed to belong to stibnite. The EDX analysis of the white area (Fig. 5c) does not prove the presence of sulfur, whereas antimony was found as a main constituent of this white area. Although the EDX signal comes not only from the surface, but also from the area close under the surface, the disappearing of the sulfur and intensive signal of antimony (Fig. 5c)) revealed the tribochemical transformation of stibnite. Österle and Urban [20] studied the composition of friction layers and friction films originated on the surface of polymer matrix composites. Although the authors do not show the chemical composition of the original composite, the chemical composition of loosened wear particles also revealed the presence of iron (major component) and antimony, they also verify the presence of another 12 elements (e.g. Cu, Zn and Sn). According to the chemical composition of wear particles we can estimate that the studied, real brake pad consists of more components than our laboratory-prepared sample. The authors used TEM/EDX/SAED technique for investigation cross sectional cuts of tested composites which provide the information about the structure, chemical and phase composition of thin friction films. Using this technique the authors observed cooper and iron oxides as well as $CuFeO_2$ and others, authors did not observed any phase containing antimony.

Filip et al. [13] discussed friction layer formation of the friction composites containing iron and copper particulates, stibnite, molybdenite, graphite, vermiculite, zircon and phenolic resin as a binder. Using XRD analysis they proved that the stibnite disappears if the temperature during friction tests reached 400°C, and they did not observe any antimony oxide even if the temperature during friction tests reached 700°C. If the same sample was heated in a temperature chamber of a compression tester under the applied load of approximately 5 MPa, the stibnite was identified even if the temperature reached 700°C and Sb_2O_4 was identified where the temperature reached 500°C. They observed that after the stibnite is decomposed the antimony alloyed copper; authors observed no formation of elemental antimony.

3.2. Differential thermal analysis

DTA curve of the mechanical mixture S1 as well as DTA curves of the original Fe and Sb_2S_3 powders obtained during heating period up to 650°C is shown in Fig 6a).

Using the Sb-S-Fe ternary diagram, rather than its isothermal cuts, we can evaluate phase composition of the mechanical mixture Fe+Sb_2S_3 during the DTA experiment. Theoretically if the mixture S1 is heated up to 540°C in inert atmosphere it can consist of Fe, FeS and $Fe_{1.27}Sb$ (ε-FeSb) [21].

On the DTA curve of Sb_2S_3 (Fig. 6a) the endothermic peak with the maximum at the temperature of 530°C appears, and may be attributed to the stibnite melting. This peak is not observable on the DTA curve of the S1 mixture. On the DTA curve of the pure iron powder no peaks were observed (Fig. 6a). During the heating of the S1 mechanical mixture one significant broad peak appears in the interval between 360–495°C. With the aim to reveal the nature of this broad peak, the initial S1 mixture was again subjected to the DTA analysis in an inert atmosphere up to i) 350°C (S1_350) and ii) 500°C (S1_500), respectively. The S1_350, S1_500 samples were analyzed using the XRD and the changes in phase composition were revealed (Fig. 6b). The initial mechanical mixture S1 consists of both constituents – Fe and Sb_2S_3. The heating of the S1 mixture up to 350 °C led obviously to the formation of elemental antimony, however presence of iron sulfide was not observed. If the mixture S1 was heated up to 500°C the diffraction peaks belonging to antimony disappeared and the diffraction peaks belonging to the ε-FeSb phase newly appeared and the diffraction peaks belonging to iron sulfide become evident.

3.3. X-ray diffraction analysis of friction layers

The X-ray diffraction patterns of the SM_0 and the SM_Al composites tested at selected temperatures of cast iron disc is shown in Fig. 7 and Fig. 8, respectively. The measurement in Brag-Brentano geometry caused that the primary beam penetrates deeply under the surface (in the order of the tenths of microns) and the registered diffraction pattern does not reflect only the phase composition of the friction surface.

The diffraction lines belonging to the crystalline raw materials used for the preparation of SM_0 and SM_Al samples, respectively appear on the diffraction patterns registered for samples tested at 100°C (Fig. 7 and 8). Fe_3O_4 is the typical oxide formed on the friction surface of friction composites containing iron, or could be the result of the secondary oxidation appearing during the storage of the composite for XRD analysis. Any changes in the phase composition were not observed after the friction test of the SM_0 sample even at 350°C (Fig. 7). The significant changes in phase composition after the friction test were observed for

the SM_Al sample (Fig. 8). When the rotor was heated up to 200°C, the diffraction lines belonging to the phase ε-FeSb were identified, whereas the intensity of these lines increases with the temperature. At the rotor temperature of 200°C, the diffraction peaks belonging to elemental Sb start to occur, and their intensity reaches a maximum at 350°C. At 350°C the diffraction lines belonging to the $FeSb_2$ phase are clearly observable. The theoretical positions of the selected diffraction lines belonging to Sb_2O_3, Sb_2O_4 and Sb_2O_5 are marked by numbers 8, 9 and 10 respectively in Fig. 7 and Fig. 8 and are emphasized by dashed vertical lines. It could be concluded that any of the well crystalline forms of antimony oxides is not presented on the friction surface of the tested samples SM_0 and SM_Al.

3.4. Thermodynamic consideration of tribochemical reaction of stibnite

The temperature dependence of the Gibbs free energy ($\Delta G=f(T)$) of the selected reactions was calculated using software HSC Chemistry 6 [22] and is pictured in Fig. 9.

The relations $\Delta G=f(T)$ is one of the criterions which show if the reaction is possible from thermodynamic point of view. This relation revealed the reaction of Sb_2O_3 with Sb_2S_3 (R5) as impossible at temperatures up to 400°C. On the other hand the reaction of Sb_2O_4 with carbon (R6) became possible at temperatures higher than 400°C (the reaction can proceed at approx. 360°C, but the rate will be very slow). The most favorable is the reaction of stibnite with oxygen giving the Sb_2O_3 (R2), followed with the reaction of iron with oxygen giving Fe_3O_4 (R3), whereas the values of ΔG for reactions R2 and R3 increase with the temperature. Metallic antimony can be obtained by the reactions of Fe with Sb_2S_3 (R1) and by the reaction of Fe with Sb_2O_3 (R4). The change of Gibbs free energy is negative for both reactions and thus the reactions R1 and R4 are thermodynamically possible, whereas the values of ΔG are decreasing with the temperature for both reactions.

With respect to reactions mentioned above, the simplified mechanism of stibnite transformation during the friction process can be outlined. At the beginning of contact of the rotor with the friction composite the absorbed oxygen reacts with stibnite to form antimony trioxide. The fact that Sb_2O_3 was not identified on the diffraction patterns of the composites after the friction test supports the theory that the antimony trioxide further reacts with iron to form iron oxide and metallic antimony. In the pure oxygen environment the direct reaction of iron and stibnite giving metallic antimony and iron sulfide can proceed. The metallic antimony then forms alloy with iron which resulted in formation of ε-FeSb and $FeSb_2$ phases.

We supplied the data showing the issue of the stibnite in semi-metallic friction composites in a more complex manner.

Conclusion

Using the data obtained with a combination of SEM-EDX, DTA, and XRD the following conclusions can be proposed:

1. The character of the friction surface significantly differs for the composite with and without the alumina abrasives. On the sample without the abrasive (SM_0), the primary contact plateaus presented by the steel wool cover the prevailing part of the friction surface. ON the sample with alumina (SM_Al), the iron primary contact plateaus are extensively covered with stibnite, which is easily transferred from stibnite raw particles due to the abrasion caused by the presence of the alumina abrasives.

2. Stibnite can react with oxygen adsorbed on the surface of the friction counterparts to form Sb_2O_3. The presence of the excess of iron causes the reaction of antimony trioxide with iron giving the metallic antimony. The direct reaction of iron with stibnite giving the metallic antimony is also thermodynamically possible.

3. The reaction of Sb_2O_3 with Sb_2S_3 giving metallic antimony is not possible at lower temperatures.

4. The presence of steel wool is the main reason for origination of the elemental antimony. Metallic antimony subsequently alloys powderized iron, what was proven by the presence of ε-FeSb and $FeSb_2$ phases.

5. The presence of any form of antimony oxide was not credibly proven at the friction surface of composites with as well as without alumina abrasives.

The results given in the manuscript are valid for the composition of the studied composites prepared in a laboratory scale. Further research dealing with the stibnite transformation in commercial semi-metallic friction composites should continue. The detailed phase analysis of the wear debris released during the friction tests of the semi-metallic friction composites containing iron and stibnite could bring new relationships between stibnite transformation occurring on the friction surface and possible formation of antimony oxides.

Acknowledgement

Financial supports from the Ministry of Education of the Czech Republic (projects ME10121, CZ.1.05/2.1.00/01.0040), National Natural Science Foundation of China 50673012 and Sino-Czech Cooperation Project (39-9) are gratefully acknowledged. The authors would like to thank Daniel Casten for language corrections.

References

[1] Y. Lu, C. Tang, M. Wright, Optimization of a commercial brake pad formulation, J. Appl. Polym. Sci. 84 (2002) 2498 - 2504.

[2] V.M. Kryachek, Friction composites: Traditions and new solutions (review). I. Powder materials, Powder Metall. Met. Ceram. 43 (2004) 581-592.

[3] P.J. Blau, Compositions, functions, and testing of friction brake materials, Technical report by oak ridge national laboratory, Tennessee, 2001.

[4] D. Chan, G.W. Stachowiak, Review of automotive brake friction materials, Proc. Inst. Mech. Eng. Part D-J. Automob. Eng. 218 (2004) 953-966.

[5] M. Eriksson, F. Bergman, S. Jacobson, On the nature of tribological contact in automotive brakes, Wear 252 (2002) 26-36.

[6] M. Eriksson, J. Lord, S. Jacobson, Wear and contact conditions of brake pads: dynamical in situ studies of pad on glass, Wear 249 (2001) 272-278.

[7] M. Kristkova, P. Filip, Z. Weiss, R. Peter, Influence of metals on the phenol-formaldehyde resin degradation in friction composites, Polym. Degrad. Stabil. 84 (2004) 49–60.

[8] A. L. Cristol-Bulthé, Y. Desplanques, G. Degallaix, Y. Berthier, Mechanical and chemical investigation of the temperature influence on the tribological mechanisms occurring in OMC/cast iron friction contact, Wear 264 (2008) 815-825.

[9] H. Jang, S. J. Kim, The effects of antimony trisulfide (Sb2S3) and zirconium silicate (ZrSiO4) in the automotive brake friction material on friction characteristics, Wear 239 (2000) 229-236.

[10] M. H. Cho, J. Ju, S. J. Kim, H. Jang, Tribological properties of solid lubricants (graphite, Sb2S3, MoS2) for automotive brake friction materials, Wear 260 (2006) 855-860.

[11] A. Wirth, R. Whitaker, An energy dispersive x-ray and imaging x-ray photoelectron spectroscopical study of transfer film chemistry and its influence on friction coefficient, J. Phys. D-Appl. Phys. 25 (1982) A38-A43.

[12] K. Hanusch, K. A. Herbst, G. Rose, H. U. Wolf, Antimony, Handbook of extractive metallurgy. vol. 2, Wiley-VCH, Weinheim, 1997, 823-844.

[13] P. Filip, Z. Weiss, D. Rafaja, On friction layer formation in polymer matrix composite materials for brake applications, Wear 252 (2002) 189-198.

[14] S. J. Kim, M. H. Cho, K. H. Cho, H. Jang, Complementary effects of solid lubricants in the automotive brake lining, Tribol. Int. 40 (2007) 15-20.

[15] H. Remy, Lehrbuch der Anorganischen Chemie, Band I. Akademische Verlagsgesellschaft Geest & Portig K.-G., Leipzig, 1957.

[16] P. Baláž, L. Takacs, E. Godočíková, I. Škorvánek, J. Kováč, W.S. Choi, Preparation of nanosized antimony by mechanochemical reduction of antimony sulphide Sb2S3, J. Alloy. Compd. 434-435 (2007) 773-775.

[17] O. von Uexküll, S. Skerfving, R. Doyle, M. Braungart. Antimony in brake pads-a carcinogenic component? J. Clean Prod. 13 (2005) 19-31.

[18] A. Iijima, K. Sato, K. Yano, H. Tago, M. Kato, H. Kimura, N. Furuta. Particle size and composition distribution analysis of automotive brake abrasion dusts for the evaluation of antimony sources of airborne particulate matter. Atmos. Environ. 41 (2007) 4908-4919.

[19] International Agency for Research on Cancer (IARC). Antimony trioxide and antimony trisulfide. In: IARC, editor. IARC Monographs. Lyon (France): IARC; 1989. p. 291.

[20] W. Österle, I. Urban. Friction layers and friction films on PMC brake pads. Wear. 257 (2004) 215-226.

[21] Diagram No. 1101408. Alloy Phase Diagrams Center. *ASM International* [online]. c2007. http://www1.asminternational.org/asmenterprise/APD/

[22] HSC Chemisty 6 [software], version 6.12, Outokumpu Technology, Pori, Finland (2006).

Figure captions:

Fig. 1. SEM image of a) iron and b) stibnite powder used for preparation of mixture S1.

Fig. 2. Temperature dependency of COF measured for samples SM_0 and SM_Al.

Fig. 3. Overall view on the friction surface of the samples: a) SM_0 and b) SM_Al tested at 350°C.

Fig. 4. a) Raw stibnite particle observed on the friction surface of the sample SM_Al tested at 350°C; b) corresponding EDX spectrum acquired from the marked area.

Fig. 5. a) Detail of the friction layer originated on the friction surface of the sample SM_Al after the friction test at 350°C; b) and c) EDX spectrum of the dark and the white areas, respectively.

Fig. 6. a) The DTA curves for Fe and Sb_2S_3 raw components and the S1 mechanical mixture; b) diffraction patterns of the initial S1 mixture, S1 after heating up to 350 (S1_350) and 500 °C (S1_500), respectively, where, 1 … Fe, 2 … Sb_2S_3, 3 … Sb, 4 … FeS, 5 … ε-FeSb.

Fig. 7. XRD patterns of the friction surfaces for the SM_0 samples tested at selected temperatures, where, 1 … Fe, 2 … Sb_2S_3, 3 … $CaSiO_3$, 4 … Fe_3O_4, 5 … $CaCO_3$, 6 … MgO, 7 … C, 8 … Sb_2O_3, 9 … Sb_2O_4, 10 … Sb_2O_5.

Fig. 8. XRD patterns of the friction surfaces for the SM_Al samples tested at selected temperatures, where, 1 … Fe, 2 … Sb_2S_3, 3 … $CaSiO_3$, 4 … Fe_3O_4, 5 … $CaCO_3$, 6 … MgO, 7 … C, 8 … Sb_2O_3, 9 … Sb_2O_4, 10 … Sb_2O_5, 11 … Al_2O_3, 12 … Sb, 13 … FeS, 14 … ε-FeSb, 15 … $FeSb_2$.

Fig. 9 The temperature dependency of the Gibbs free energy calculated for selected reactions:

R1: $Sb_2S_3 + 3Fe = 3FeS + 2Sb$;

R2 … $Sb_2S_3 + 4.5O_2(g) = Sb_2O_3 + 3SO_2(g)$;

R3: $3Fe + 2O_2(g) = Fe_3O_4$;

R4 … $3Fe + Sb_2O_3 = 2Sb + 3FeO$;

R5: $2\ Sb_2O_3 + Sb_2S_3 = 6Sb + 3SO_2(g)$;

R6 … $Sb_2O_4 + 4C = 2Sb + 4CO(g)$

Table 1. Relative content (vol.%) of raw materials in the prepared friction composites SM_0 and SM_Al.

Ingredient	SM_0	SM_Al
Steel wool	42.00	39.24
Oxidized PAN fiber	7.70	7.19
Wollastonite	3.00	2.80
Stibnite	4.80	4.48
Coke	3.00	2.80
$Ca(OH)_2$	0.70	0.65
$CaCO_3$	3.00	2.80
MgO	1.10	1.03
NBR	20.10	18.81
Phenolic resin	14.60	14.6
Al_2O_3	-	5.6

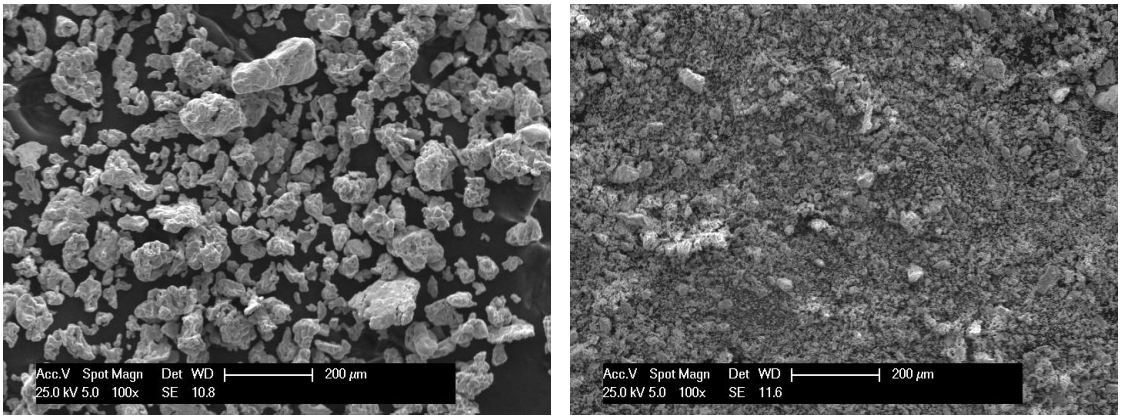

Fig. 1. SEM image of a) iron and b) stibnite powder used for preparation of mixture S1.

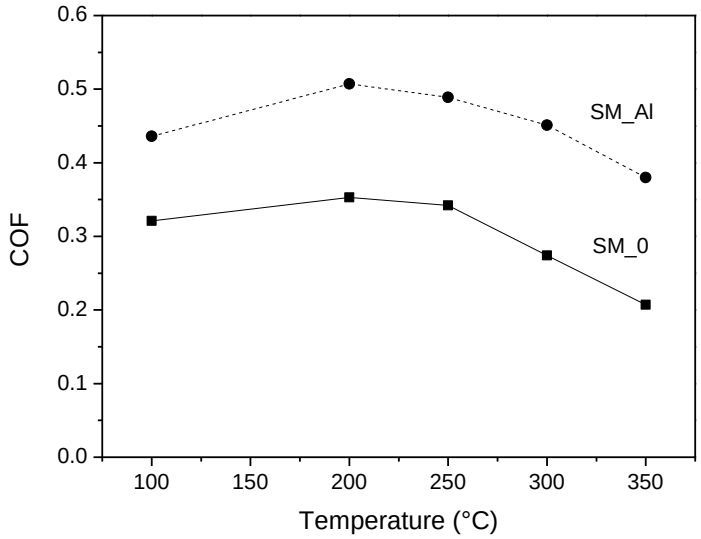

Fig. 2. Temperature dependency of COF measured for samples SM_0 and SM_Al.

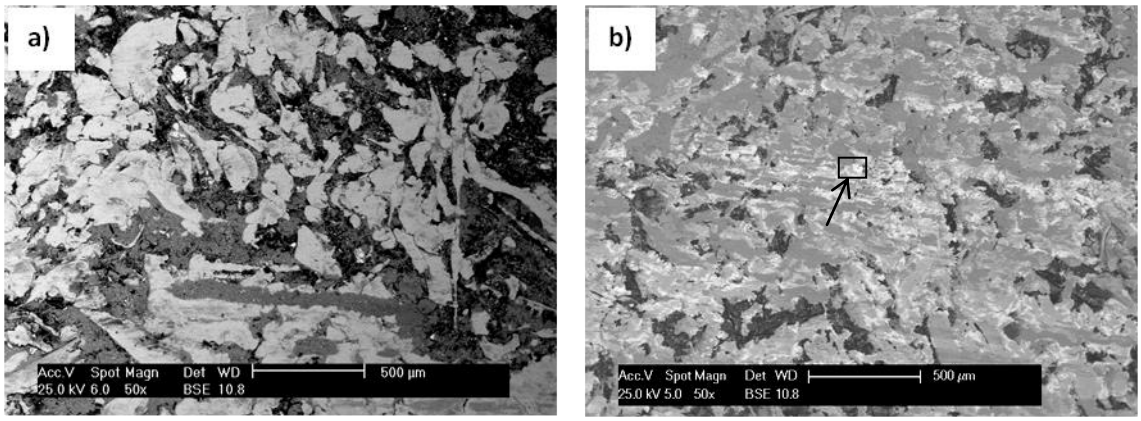

Fig. 3. Overall view on the friction surface of the samples: a) SM_0 and b) SM_Al tested at 350°C.

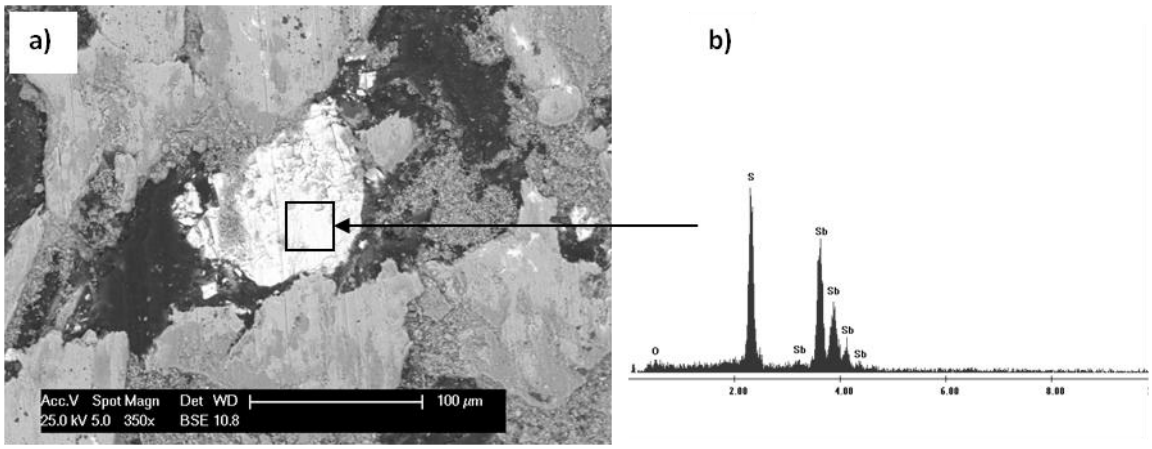

Fig. 4. a) Raw stibnite particle observed on the friction surface of the sample SM_Al tested at 350°C; b) corresponding EDX spectrum acquired from the marked area.

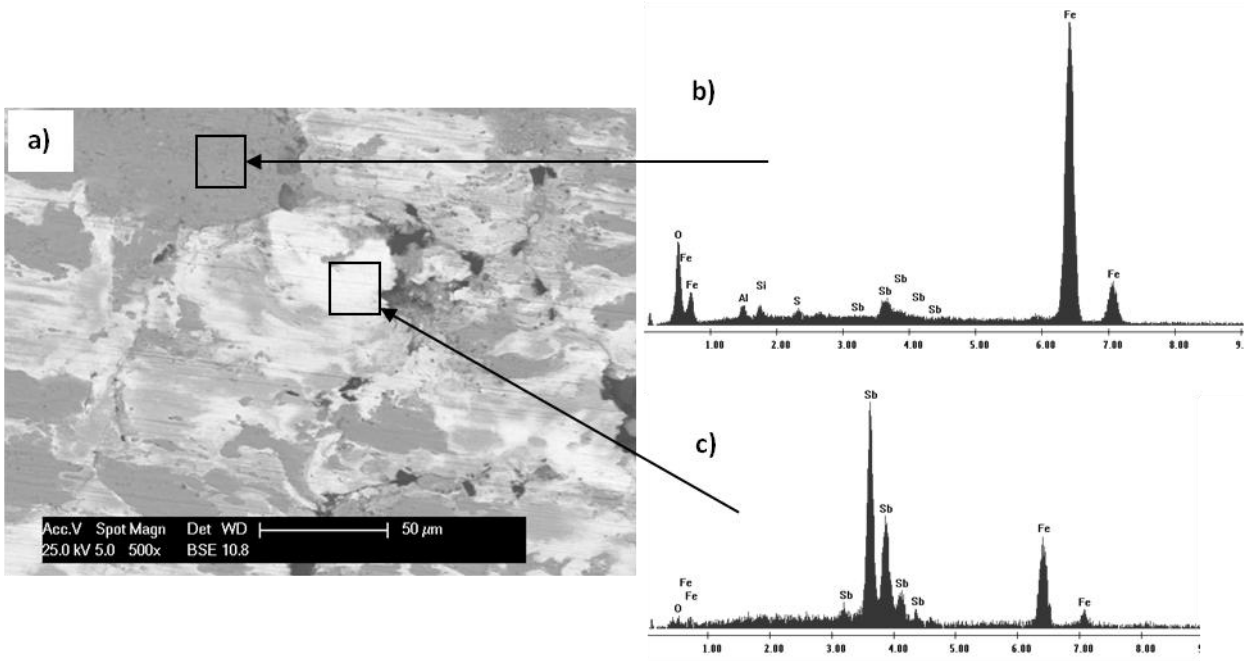

Fig. 5. a) Detail of the friction layer originated on the friction surface of the sample SM_Al after the friction test at 350°C; b) and c) EDX spectrum of the dark and the white areas, respectively.

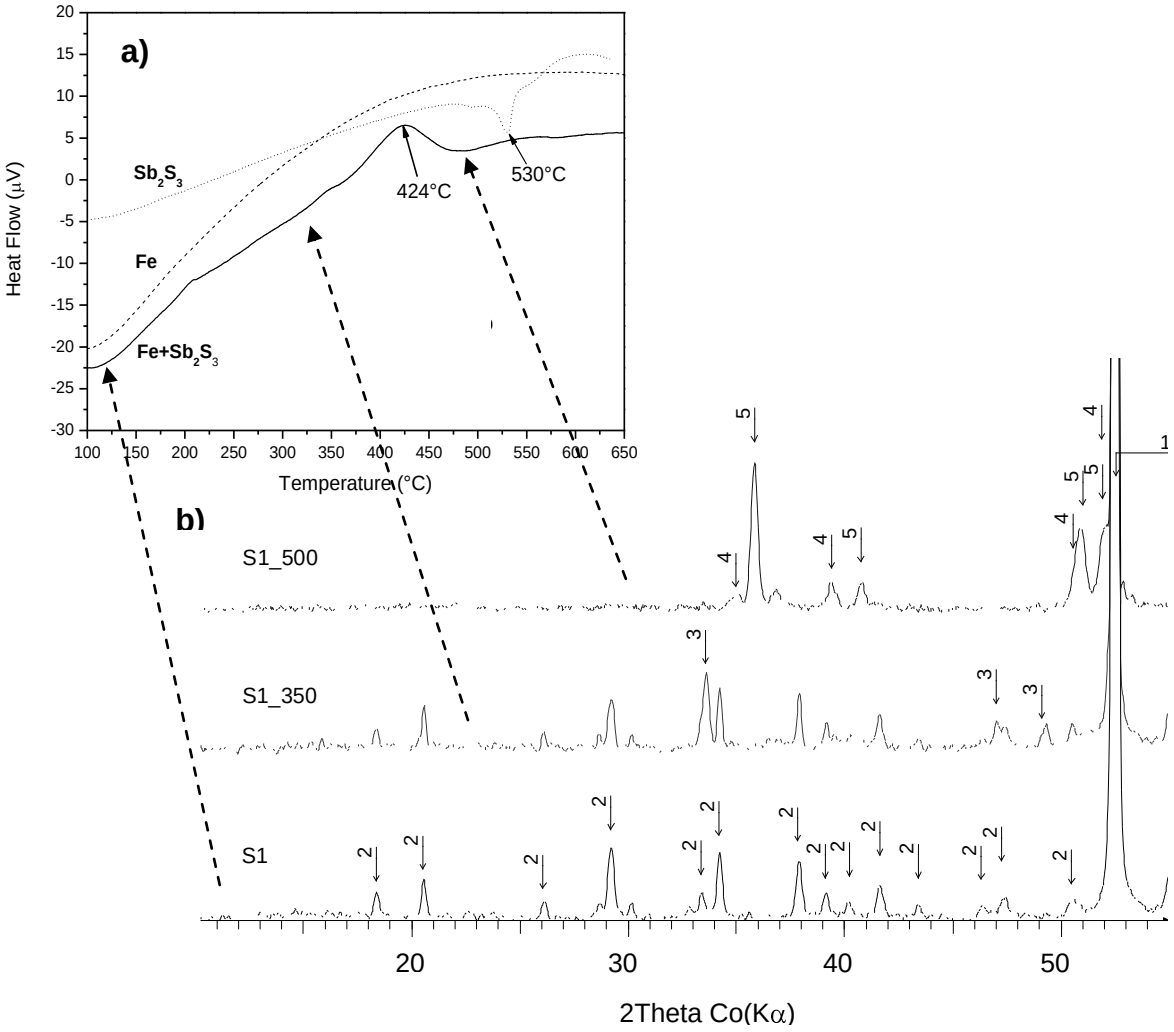

Fig. 6. a) The DTA curves for Fe and Sb_2S_3 raw components and the S1 mechanical mixture; b) diffraction patterns of the initial S1 mixture, S1 after heating up to 350 (S1_350) and 500 °C (S1_500), respectively, where, 1 … Fe, 2 … Sb_2S_3, 3 … Sb, 4 … FeS, 5 … ε-FeSb.

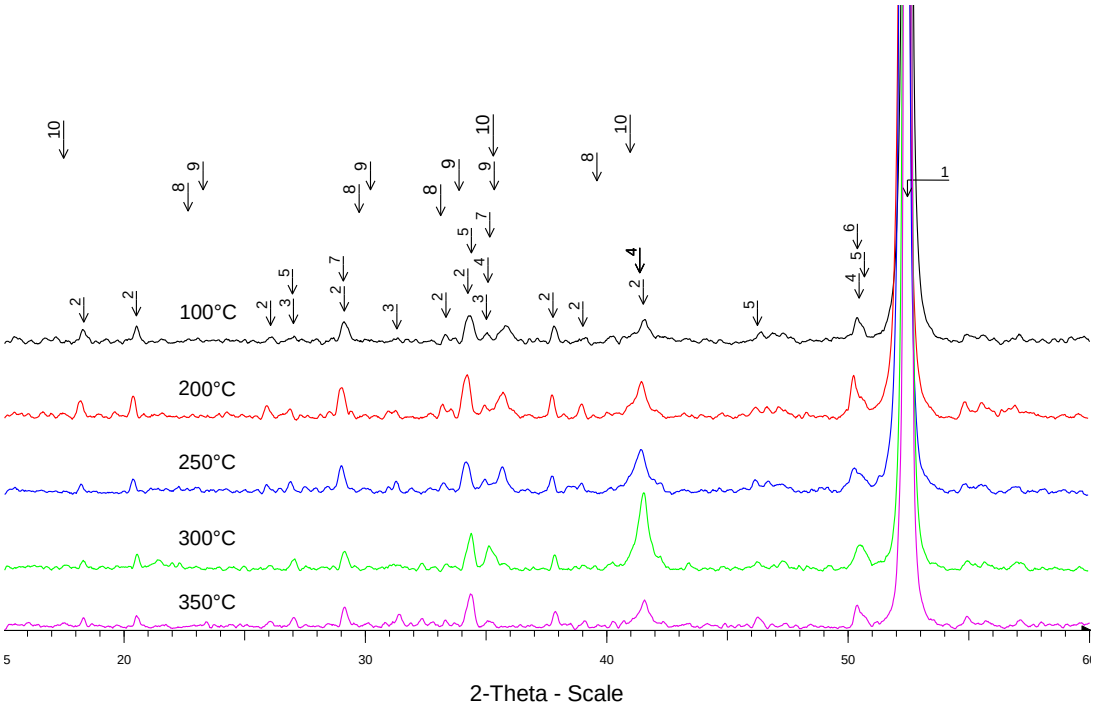

Fig. 7. XRD patterns of the friction surfaces for the SM_0 samples tested at selected temperatures, where, 1 … Fe, 2 … Sb_2S_3, 3 … $CaSiO_3$, 4 … Fe_3O_4, 5 … $CaCO_3$, 6 … MgO, 7 … C, 8 … Sb_2O_3, 9 … Sb_2O_4, 10 … Sb_2O_5.

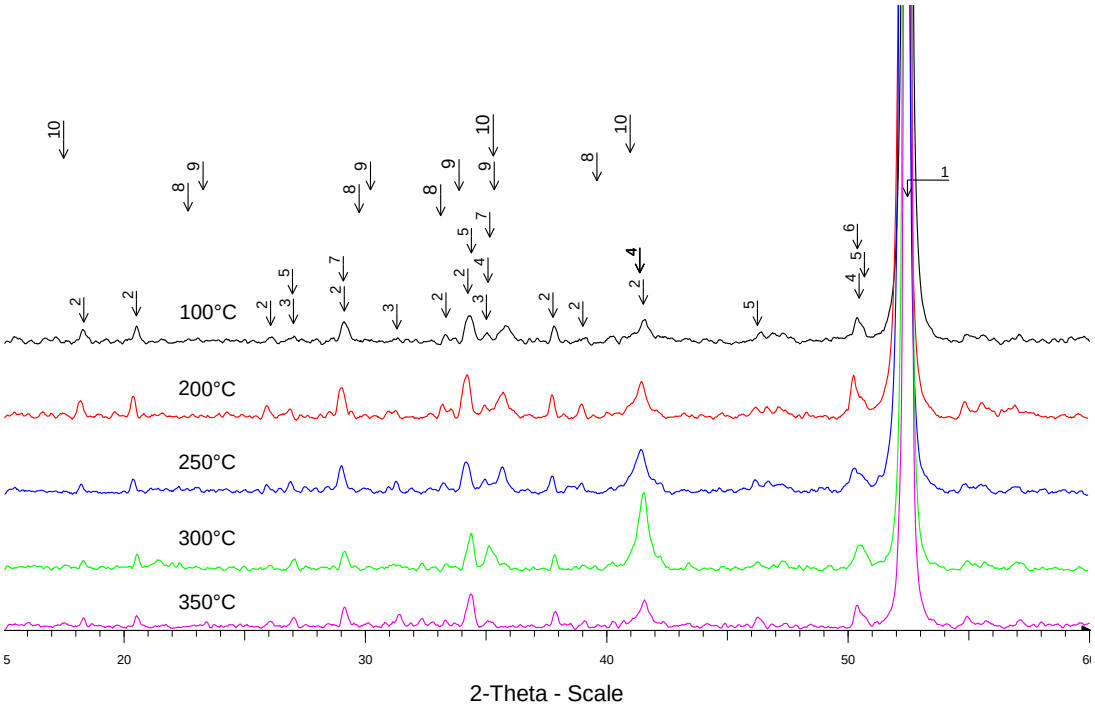

Fig. 8. XRD patterns of the friction surfaces for the SM_Al samples tested at selected temperatures, where, 1 … Fe, 2 … Sb_2S_3, 3 … $CaSiO_3$, 4 … Fe_3O_4, 5 … $CaCO_3$, 6 … MgO, 7 … C, 8 … Sb_2O_3, 9 … Sb_2O_4, 10 … Sb_2O_5, 11 … Al_2O_3, 12 … Sb, 13 … FeS, 14 … ε-FeSb, 15 … $FeSb_2$.

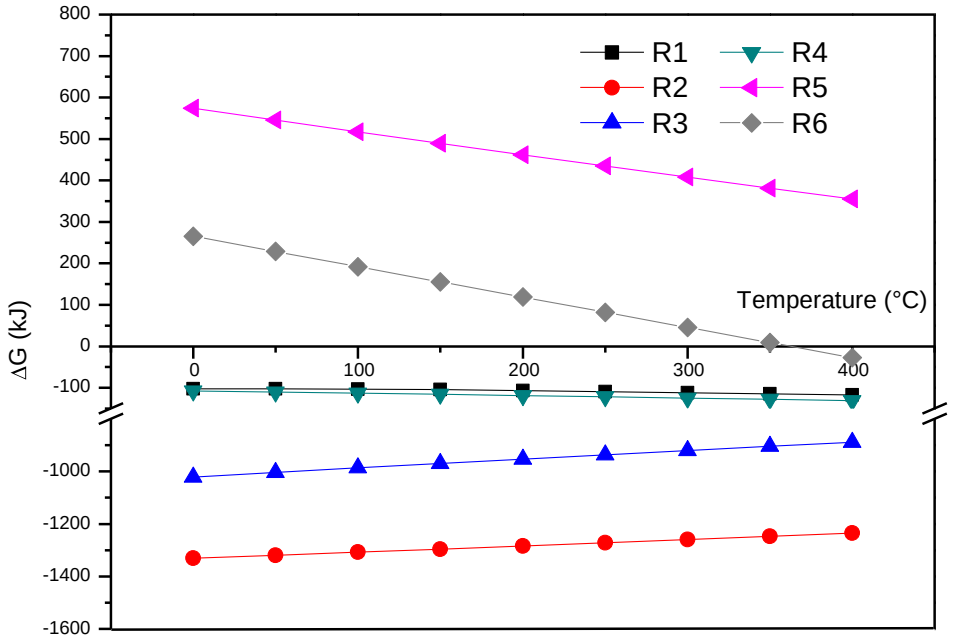

Fig. 9 The temperature dependency of the Gibbs free energy calculated for selected reactions:

R1: $Sb_2S_3 + 3Fe = 3FeS + 2Sb$;

R2 … $Sb_2S_3 + 4.5O_2(g) = Sb_2O_3 + 3SO_2(g)$;

R3: $3Fe + 2O_2(g) = Fe_3O_4$;

R4 … $3Fe + Sb_2O_3 = 2Sb + 3FeO$;

R5: $2\ Sb_2O_3 + Sb_2S_3 = 6Sb + 3SO_2(g)$;

R6 … $Sb_2O_4 + 4C = 2Sb + 4CO(g)$